Deciphering when Metal Corrosion is Spontaneous in Molten Fluorides Using Potential-Activity Diagrams

Ho Lun Chan[‡,*,**] *and John R. Scully*[*,**]

The work identifies the conditions for thermodynamically favored spontaneous metal corrosion using potential-activity diagrams tailored for high-temperature molten fluorides. These diagrams provide insights into the thermodynamic phase stability of both solid and dissolved metal species, such as Cr, Cr(II), Cr(III), Ni, Ni(II), Fe, and Fe(II), along with their potential primary oxidizers, including Eu(III), O_2, and HF, over a broad range of theoretical F^- anion activities. The work further examines the practical implications, prospects, and challenges associated with the construction of these diagrams. The key objective of this project is to pinpoint crucial thermodynamic variables that substantially affect metal corrosion electrochemistry in the context of molten salt nuclear reactor applications.

KEY WORDS: corrosion, electrochemistry, molten salt reactor, thermodynamics

INTRODUCTION

In the past decade, there has been a notable increase in the publication of corrosion research focused on candidate metals and alloys for Gen-IV molten salt reactor applications.[1] This trend highlights the growing interest in understanding and addressing the corrosion challenges inherent to this technology. Numerous studies have intentionally introduced oxidizers, including HF, CrF_3, and EuF_3, into the salt mixture to explore the impact of oxidizing impurities on the corrosion process, the driving force for corrosion, the rates of corrosion, and the underlying microstructural damage seen in candidate metals and alloys.[2-3] However, these studies are often conducted phenomenologically[4] and lack conceptualization of spontaneous corrosion processes explained by foundational thermodynamic and kinetics theories of corrosion.[5-7]

A step toward improving the thermodynamic foundations involves the construction and partial verification of potential-activity diagrams, similar to Pourbaix diagrams in aqueous systems. These diagrams can display the stability regions of species such as Cr, Cr(II), and Cr(III) in molten fluorides, as well as indicate the conditions necessary for the reduction of oxidizers and the occurrence of spontaneous corrosion.[8] However, earlier works were constrained to the discussion of phase stability of Cr species, presuming them to be solvated to F^- at 600°C. There is a gap in predicting and comparing oxidizer candidates in molten fluorides that can meet the conditions for spontaneous corrosion for a given metal. Specifically, which types of oxidizers, at what concentrations, and for which metals (e.g. Cr, Fe, and Ni) remain unexplored in many previous studies. Hence, the objective is to expand our original approach to define the phase stability of Ni, Fe, and other potential oxidizing elements, such as HF, O_2, Eu(III), and Cr(III) when present in low finite concentrations. When considered together these help to define the conditions for spontaneous corrosion.

EXPERIMENTAL PROCEDURES

The first assumption of this work is that the corrosion of metallic elements in molten fluorides occurs by electrochemical processes governed by mixed potential theory. Corrosion theory applied to molten fluorides states that the thermodynamic driving force for oxidative corrosion is determined by the difference in the Gibbs free energies of reaction (ΔG^o_{rxn}) present between the cathodic half-cell reduction reactions of the oxidants, coupled with half-cell anodic oxidation reactions associated with transition metals used in structural materials exposed. This difference must be negative for a reaction to occur satisfying the condition $\Delta G < 0$ for a spontaneous process given $\Delta G = -nF\Delta E$. Reaction (1) is the most general approach to describe such a half-cell reaction.[9]

$$Ox + e^- \leftrightarrow Red \quad (1)$$

In regards to the anodic reaction, metal dissolution in molten fluorides is often described by the oxidation of a pure metal to a metal fluoride species represented in Reaction (2):[2,10-12]

$$M + xF^-(ms) \leftrightarrow MF_x^{n-x}(ms) + ne^- \quad (2)$$

where (ms) indicates dissolved species in the molten salt and M represents the dissolving metallic element, including Ni, Cr, and Fe. The relative tendencies of metal dissolution depend on the ΔG^o_{rxn} of the relevant half-cell redox reactions. In the context of the cathodic reactions, hydrofluoric acid (HF), formed due to

Submitted for publication: June 30, 2023. Revised and accepted: August 14, 2023. Preprint available online: September 20, 2023, https://doi.org/10.5006/4401.
‡ Corresponding author. E-mail: hc4ry@virginia.edu.
* Department of Materials Science and Engineering, University of Virginia, 395 McCormick Rd, Charlottesville, Virginia 22903.
** Center of Electrochemical Science and Engineering, University of Virginia, 395 McCormick Rd, Charlottesville, Virginia 22903.

ISSN 0010-9312 (print), 1938-159X (online)

H_2O moisture dissociation and fluorination (3), is often in a molten salt containing this oxidant (Ox) during open-circuit corrosion leading to (4) in many studies:

$$H_2O(g) + 2F^-(ms) \leftrightarrow 2HF(g) + O^{2-}(ms) \quad (3)$$

$$HF(ms) + e^- \leftrightarrow \frac{1}{2}H_2(g) + F^-(ms) \quad (4)$$

Other relevant oxidizers toward spontaneous corrosion studied include reduction of oxygen gas (O_2) via (5) and europium (III) fluoride (EuF_3) via (6):[13-14]

$$O_2(g) + 4e^- \leftrightarrow 2O^{2-}(ms) \quad (5)$$

$$EuF_3(ms) + e^- \leftrightarrow EuF_2(ms) + F^-(ms) \quad (6)$$

Metallic corrosion products, such as CrF_3 or more generally Cr(III), can also act as oxidizers during spontaneous corrosion of structural metals, reducing to a lower oxidation state such as CrF_2 or Cr(II) when a sufficient driving force is present:

$$CrF_3(ms) + e^- \leftrightarrow CrF_2 + F^-(ms) \quad (7)$$

The driving forces pertaining to these half-cell redox reactions under nonunity activity can be described by first writing the Nernst equation for each participating half-cell reaction (8):

$$E_{redox} = E^0_{redox} - \frac{2.303RT}{nF}\log\left(\frac{a_{red}}{a_{ox}}\right) \quad (8)$$

where E_{redox} is the Nernst potential or activity modified standard potential for an half-cell redox reaction, R is the universal gas constant equal to 8.31 J/mol×K, T is temperature in Kelvin, n is the number of e^- transferred to complete the reaction a single time, F is the Faraday's constant of 96,500 C/mol e–, a_i (= γ_i C_i) is the ion activity, C_i is the molar concentration, and E^0_{redox} is the standard electrode potential. As an initial estimate, the activity coefficient (γ_i) of all species in this brief manuscript is assumed to be 1.

Table 1 lists the Gibbs energy of formation ($\Delta G^o_{formation}$) between 600°C and 800°C of all the species studied in this work. The Gibbs energy of fusion (ΔG^o_{fusion}) was also used in calculating the ΔG_{rxn}.[8,13] Given that most of these dissolved species are in a molten state at the evaluated temperatures, a minor adjustment via (9) was necessary. The ΔG_{rxn} can then be calculated using Equation (10) noting that v_i represents the stoichiometric number of a species, and to calculate E^0_{redox} using (11)[9] (note that these thermodynamic data were retrieved from the Factsage 13.1™† pure substance database):[15]

$$\Delta G^o_f = \Delta G^o_{fusion} + \Delta G^o_{formation} \quad (9)$$

$$\Delta G^o_{rxn} = \Sigma v_i \Delta G^o_f(Red) - \Sigma v_i \Delta G^o_f(Ox) \quad (10)$$

$$E^0_{redox} = -\frac{\Delta G^o_{rxn}}{nF} \quad (11)$$

Corrosion is spontaneous when E_{redox} for the proposed cathodic reaction is more positive than that for the corresponding anodic reaction, where upon ΔG is negative, indicating a spontaneous corrosion cell and determining the direction of each reaction (the anode gives up electrons; the cathode gains electrons). This relationship is shown in (12). Note that (12) also applies to the E^0_{redox} and that the sign of E_{redox} does not change with reaction direction.

$$E_{redox}(Cathodic) - E_{redox}(Anodic) \begin{cases} > 0, \text{spontaneous} \\ = 0, \text{equilibrium} \\ < 0, \text{Not spontaneous} \end{cases} \quad (12)$$

Table 2 reports some pertinent half-cell redox reactions, the standard electrode potential, E^0_{redox}, and the activity modified or Nernst equation considered in this work. Further discussions are given below about the application of potential-activity diagrams for analysis of the propensity for spontaneous corrosion in molten LiF-NaF-KF salts (or FLiNaK) with various impurities as the assumed predominant cathodic reactions. For thermodynamic reference, it is assumed that the ΔG^o_f of F^- at 600°C is 0 and the partial pressure of all gaseous species (F_2) to be 1 atm. It was noted that metal fluoride species are represented using the Roman numeral corresponding to the positively charged cation, e.g., Cr(II) as CrF_2 and Eu(III) as EuF_3.

Table 1. *Gibbs Free Energy of Fusion and Formation for Select Chemical Compounds at 600°C*[12]

Compound	ΔG^o_{fusion} (kJ/mol)	$\Delta G^o_{formation}$ (kJ/mol) T = 600°C
F^-	–	0
O^{2-}	–	−243.4
HF	–	−277.9
EuF_3	$54.4–32 \times 10^{-3} \times T(K)$	−1,351.4
EuF_2	–	−1,046.3
NiF_2	$69–41.7 \times 10^{-3} \times T(K)$	−521.9
FeF_2	$47.4–38 \times 10^{-3} \times T(K)$	−593.2
CrF_2	$34–29.1 \times 10^{-3} \times T(K)$	−665.3
CrF_3	$229.1–183 \times 10^{-3} \times T(K)$	−891.2
KF	$28.2–25 \times 10^{-3} \times T(K)$	−481.3
LiF	$27.2–24.254 \times 10^{-3} \times T(K)$	−531.1
NaF	$33.3–26.277 \times 10^{-3} \times T(K)$	−508.3

RESULTS AND DISCUSSIONS

To construct a potential-activity diagram, the initial step involves determining an appropriate potential window. This is dictated by selecting a potential range spanning the oxidation of F^- to F_2 species and the reduction of molten LiF (or Li^+), NaF (or Na^+), and KF (or K^+) to their respective neutral metal states, as illustrated in Figure 1(a).

The lower potential boundary is set by the oxidation of metal salt cation components which will be assumed oxidized under all potentials. There are two different representations in the literature for determining the Nernst potential of salt metal cation reductions: one considers the metal fluoride compound

† Trade name.

Table 2. *A List of Half-Cell Redox Reactions, their Nernst Potential Equation and Formal Potentials (E^0) Calculated at 600°C Utilized in This Work*[12]

Half-Cell Redox Equation	Nernst Equation/Gibbs Free Energy Expression	E^0_{redox} (vs. F_2/F^-)
$F_2 + 2e^- \leftrightarrow 2F^-$	$E = E^0 - \frac{2.303RT}{2F}\log\left(\frac{a^2_{F^-}}{p_{F_2}}\right)$	0
$O_2 + 4e^- \leftrightarrow 2O^{2-}$	$E = E^0 - \frac{2.303RT}{4F}\log\left(\frac{a^2_{O^{2-}}}{p_{O^2}}\right)$	−1.261
$HF + e^- \leftrightarrow \frac{1}{2}H_2 + F^-$	$E = E^0 - \frac{2.303RT}{F}\log\left(\frac{p^{1/2}_{H_2}a_{F^-}}{a_{HF}}\right)$	−2.880
$EuF_3 + e^- \leftrightarrow EuF_2 + F^-$	$E = E^0 - \frac{2.303RT}{F}\log\left(\frac{a_{EuF_2}a_{F^-}}{a_{EuF_3}}\right)$	−2.894
$Ni + 2F^- \leftrightarrow NiF_2 + 2e^-$	$E = E^0 + \frac{2.303RT}{2F}\log\left(\frac{a_{NiF_2}}{a^2_{F^-}}\right)$	−2.536
$Fe + 2F^- \leftrightarrow FeF_2 + 2e^-$	$E = E^0 + \frac{2.303RT}{2F}\log\left(\frac{a_{FeF_2}}{a^2_{F^-}}\right)$	−3.000
$Cr + 2F^- \leftrightarrow CrF_2 + 2e^-$	$E = E^0 + \frac{2.303RT}{2F}\log\left(\frac{a_{CrF_2}}{a^2_{F^-}}\right)$	−3.403
$Cr + 3F^- \leftrightarrow CrF_3 + 3e^-$	$E = E^0 + \frac{2.303RT}{2F}\log\left(\frac{a_{CrF_3}}{a^3_{F^-}}\right)$	−2.430
$CrF_3 + e^- \leftrightarrow CrF_2 + F^-$	$E = E^0 + \frac{2.303RT}{2F}\log\left(\frac{a_{CrF_3}}{a_{CrF_2}a_{F^-}}\right)$	−3.078
$KF + e^- \leftrightarrow K + F^-$	$E = E^0 - \frac{2.303RT}{F}\log\left(\frac{a_{F^-}a_K}{a_{KF}}\right)$	−4.921
$K^+ + e^- \leftrightarrow K$	$E = E^0 - \frac{2.303RT}{F}\log\left(\frac{a_K}{a_{K^+}}\right)$	−4.854
$LiF + e^- \leftrightarrow Li + F^-$	$E = E^0 - \frac{2.303RT}{F}\log\left(\frac{a_{F^-}a_{Li}}{a_{LiF}}\right)$	−5.442
$Li^+ + e^- \leftrightarrow Li$	$E = E^0 - \frac{2.303RT}{F}\log\left(\frac{a_{Li}}{a_{Li^+}}\right)$	−5.379
$NaF + e^- \leftrightarrow Na + F^-$	$E = E^0 - \frac{2.303RT}{F}\log\left(\frac{a_{F^-}a_{Na}}{a_{NaF}}\right)$	−5.159
$Na^+ + e^- \leftrightarrow Na$	$E = E^0 - \frac{2.303RT}{F}\log\left(\frac{a_{Na}}{a_{Na^+}}\right)$	−5.052

(e.g., KF) as a singular entity, leveraging the more developed thermodynamic data for these species.[10] However, this approach assumes a fluoride-dependent reaction, which remains a subject of debate and requires further experimental validation. The other assumes a fully ionized form (e.g., K^+).[6]

At the vertical dashed line (representing F^- activity of FLiNaK), a substantial difference in potential of roughly 500 mV between KF/K and K^+/K is observed (Figure 1[a]). This implies that the K^+/K reaction is thermodynamically more inclined to occur. However, this may not be the case for salts with a low F^- activity. Given this comparison, K^+/K will be considered as the lower potential boundary of FLiNaK salts in the subsequent discussion.

Figure 1(b) shows half-cell redox reactions involving gas generation and consumption if present. For instances, F^- is reduced to form F_2, HF to form H_2, and O^{2-} to form O_2. Shaded regions represent stability fields dominated by the evolution of specific gas species. Concentrations of HF and O^{2-} between 10 ppm and 1,000 ppm are considered. These are likely cathodic reactions when coupled with metal oxidation in molten salts.

Other cathodic oxidations include the reduction of Cr(III) to Cr(II) or Ni(II) to Ni if NiF_2 is present in the molten fluorides. For spontaneous metal dissolution, the potential should fall within these regions, typically aligned with H_2 gas evolution. Metals with half-cell electrode potentials in the gray region will not corrode spontaneously unless an additional oxidizer like Eu(III) is present. The role of O_2 as an oxidizer has not been investigated in detail due to uncertainties surrounding its solubility in FLiNaK at 600°C and the possibility for it to be oxidized by F^- to form O^{2-}.[14]

Figure 2 demonstrates the spontaneity and relative driving forces for the dissolution of pure Ni, Fe, and Cr. As expected, the Nernst potentials of Ni/Ni(II), Fe/Fe(II), and Cr/Cr(II) follow a descending order corresponding to the nobility of each element. Selected cathodic half-cell reactions are included in Figure 2 for this discussion of possible corrosion cells that might form. In order for a reaction to be spontaneous, the cathodic reaction (e.g., HF/H_2, Eu(III)/Eu(II)) must possess a more positive Nernst potential than its anodic counterparts. Fe/Fe(II) and Cr/Cr(II) exhibit lower Nernst potentials compared to

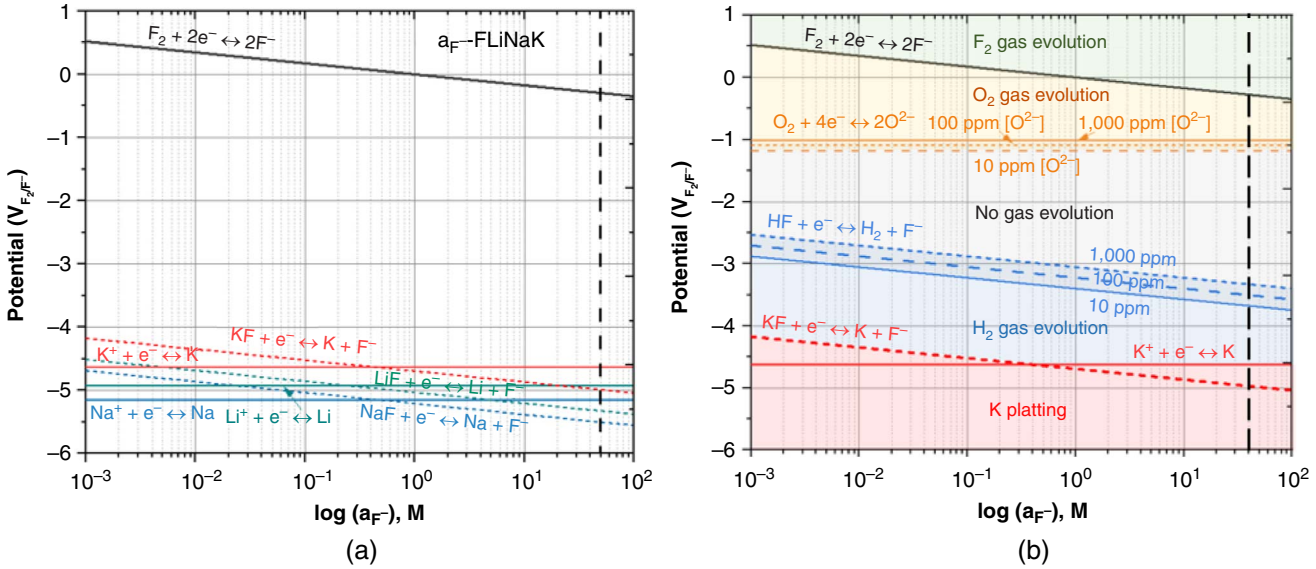

FIGURE 1. *Potential-fluoride activity diagrams at 600°C (a) shows the potential stability window defined by the fluorine gas evolution (F_2/F^-) and stability in the oxidized state for Li^+, K^+, and Na^+ cation constituents. The vertical dashed line indicates the F^- activity in FLiNaK salt at a_{F^-} = 49.3 M and (b) displays the Nernst potentials of O_2/O^{2-} and HF/H_2 reactions assuming the oxidant concentration of 10 ppm, 100 ppm, and 1,000 ppm. The diagram was shaded with different colors to indicate the type of gas evolution and/or platting of salt cations within the phase stability map.*

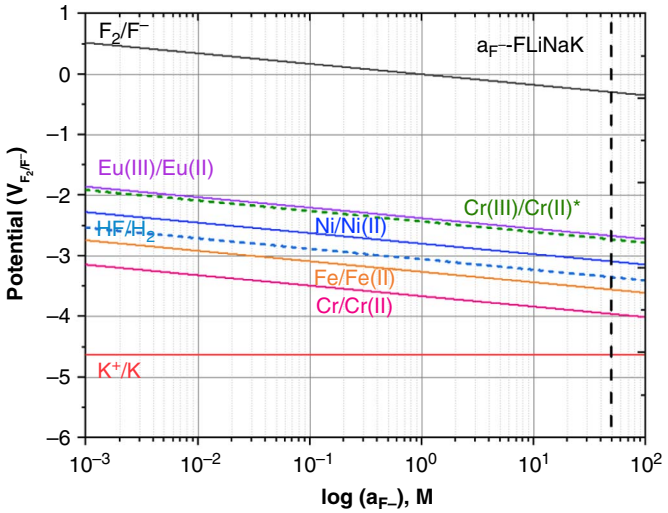

FIGURE 2. *Potential-fluoride activity diagrams displaying the Nernst potentials of F_2/F^- O_2/O^{2-}, Eu(II)/Eu(III), Ni/Ni(II), HF/H_2, Fe/Fe(II), Cr/Cr(II), Cr(II)/Cr(III), K/K^+, and half-cell redox reactions calculated at 600°C. The concentration of O^{2-} and HF was assumed to be 1,000 ppm (corresponding to the molar concentration of 1.00×10^{-1} M and 1.25×10^{-1} M), Cr(II) in Cr(II)/Cr(III) and Eu(II) are taken to be 10^{-6} M, while that of Eu(III), Ni(II), Fe(II), and Cr(II) in Cr/Cr(II) are assumed to be 10^{-3} M.*

HF/H_2 (at 1,000 ppm), indicating the prevalence of impurity-driven corrosion in the presence of trace water.[1,16] Conversely, Ni/Ni(II) displays a higher potential than HF/H_2, suggesting potential immunity to HF-driven attack.[10] These two observations align with published experimental observations.[1] During spontaneous metal corrosion, the thermodynamic and kinetic factors associated with their respective cathodic and anodic reactions establish a mixed potential, typically termed the corrosion potential. Further interpretation is provided in Pizzini and Morlotti.[14] It should be noted that Fe(III) and Ni(III) were not plotted, but they are other possible species to consider in corrosion cells.

The reduction of higher valence cations, such as Eu(III) and Cr(III), which also act as oxidizers, is hypothetically capable of oxidizing all three elements Ni-, Cr-, or Fe-based on the imposed assumption. Additionally, for Cr, fluoride complexes such as CrF_3^- for Cr(II) and CrF_6^{3-} in the case of Cr(III) may also form (and change the electrode potential) as suggested by both experimental and computational studies.[8,17] The effect of fluoride complex formation on these Cr-F phase stability diagrams was investigated in our previous work.[8]

Our discussion herein of this work highlights some of the further research required to address various underlying assumptions. Factors such as activity coefficients, ratios between higher and lower valence states, fluoride complex formation, and the possibility of saturation all require thorough investigation. Moreover, substrate effects can change thermodynamic driving forces. Crystal orientation and nanocurvature can also affect the standard electrode potential.[18-19] However, this work provides a foundation for understanding the spontaneity of metal corrosion in terms of phase stability diagrams. The authors' latest work demonstrates the practicality of these diagrams in understanding experimental polarization curves.[6] Beyond these insights, the work also establishes a thermodynamic framework that facilitates deeper comprehension of the contributory factors to corrosion, such as radiation.

CONCLUSIONS

➢ This study utilizes potential-activity diagrams tailored for molten fluorides, designed to report in graphical form the driving forces behind various half-cell redox reactions forming a spontaneous corrosion cell involving one or more anodic and cathodic half-cell reactions. Such diagrams enable a comprehensive understanding of phase stability for different metal species and their potential predominant oxidizers during corrosion (e.g., Eu(III), O_2, and HF) assuming a hypothetical range

of fluoride activities. However, the study recognizes certain assumptions embedded within this framework and those require further experimental validation. Moreover, the diagram represents an equilibrium condition and does not inform corrosion kinetics. This framework could potentially predict conditions for spontaneous corrosion and serves as a tool for devising strategies for corrosion control and mitigation in these challenging environments, contributing to materials sustainability in fourth generation molten salt reactor technologies.

ACKNOWLEDGMENTS

This work was supported as part of FUTURE (Fundamental Understanding of Transport Under Reactor Extremes), an Energy Frontier Research Center funded by the U.S. Department of Energy, Office of Science, Basic Energy Sciences. H.C. acknowledges the National Science Foundation Graduate Research Fellowship Program under Grant No. #1842490. Any opinions, findings, conclusions, or recommendations expressed in this material are those of the author(s) and do not necessarily reflect the views of the U.S. Department of Energy nor the National Science Foundation.

References

1. S. Guo, J. Zhang, W. Wu, W. Zhou, *Prog. Mater. Sci.* 97 (2018): p. 448-487.
2. Y.L. Wang, Q. Wang, H.J. Liu, C.L. Zeng, *Corros. Sci.* 103 (2016): p. 268-282.
3. S.W. McAlpine, N.C. Skowronski, W. Zhou, G. (Tony) Zheng, M.P. Short, *J. Nucl. Mater.* 532 (2020): p. 151994.
4. M. Hong, H.L. Chan, Y. Xie, E. Romanovskaia, J.R. Scully, P. Hosemann, *Corros. Sci.* 212 (2023): p. 110913.
5. D. Sulejmanovic, J.M. Kurley, K. Robb, S. Raiman, *J. Nucl. Mater.* 553 (2021): p. 152972.
6. H.L. Chan, E. Romanovskaia, V. Romanovski, M. Hong, D. Sur, P. Hosemann, J.R. Scully, *J. Electrochem. Soc.* 170, 8 (2023): p. 081502.
7. M. Hong, H.L. Chan, J.R. Scully, P. Hosemann, *J. Nucl. Mater.* 584 (2023): p. 154548.
8. H.L. Chan, E. Romanovskaia, J. Qiu, P. Hosemann, J.R. Scully, *npj Mater. Degrad.* 6 (2022): p. 46.
9. D.A. Jones, *Principles and Prevention of Corrosion* (Hoboken, NJ: Prentice Hall, 1996).
10. J. Zhang, C.W. Forsberg, M.F. Simpson, S. Guo, S.T. Lam, R.O. Scarlat, F. Carotti, K.J. Chan, P.M. Singh, W. Doniger, K. Sridharan, J.R. Keiser, *Corros. Sci.* 144 (2018): p. 44-53.
11. Y. Liu, Y. Song, H. Ai, M. Shen, H. Liu, S. Zhao, Y. Liu, Z. Fei, X. Fu, J. Cheng, *Corros. Sci.* 169 (2020): p. 108636.
12. L. Massot, M. Gibilaro, D. Quaranta, P. Chamelot, *J. Electrochem. Soc.* 168 (2021): p. 026510.
13. S. Guo, N. Shay, Y. Wang, W. Zhou, J. Zhang, *J. Nucl. Mater.* 496 (2017): p. 197-206.
14. S. Pizzini, R. Morlotti, *Electrochim. Acta* 10 (1965): p. 1033-1041.
15. C.W. Bale, E. Bélisle, P. Chartrand, S.A. Decterov, G. Eriksson, K. Hack, I.-H. Jung, Y.-B. Kang, J. Melançon, A.D. Pelton, C. Robelin, S. Petersen, *CALPHAD* 33 (2009): p. 295.
16. Q. Liu, H. Sun, H. Yin, L. Guo, J. Qiu, J. Lin, Z. Tang, *Corros. Sci.* 160 (2019): p. 108174.
17. N. Winner, H. Williams, R.O. Scarlat, M. Asta, *J. Mole. Liq.* 335 (2021): p. 116351.
18. C.D. Taylor, P. Lu, J. Saal, G.S. Frankel, J.R. Scully, *npj Mater. Degrad.* 2 (2018): p. 6.
19. E. Romanovskaia, H.L. Chan, V. Romanovski, F. Garfias, M. Hong, S. Mastromarino, P. Hosemann, R. Scarlat, J.R. Scully, *Corros. Sci.* 222 (2023): p. 111389.